Mahmoud Rostami Varnousfaaderani
Mohammad Javad Ketabdari

ISSN 1333-1124
eISSN 1849-1391

APPLICATION OF THE MODIFIED WEAKLY COMPRESSIBLE SPH METHOD TO THE 3D TURBULENT WAVE BREAKING IMPACT

Summary

In this paper, the mesh-less weakly compressible Smoothed Particle Hydrodynamics (SPH) method was used to solve the continuity and momentum equations with laminar viscosity and the sub-particle scale (SPS) turbulence model. To correct the pressure field and improve the accuracy of free surface, modification of the kernel and its gradient is applied to weakly compressible SPH. The modified method, namely the mSPH-T-K, was also equipped with periodic smoothing of the density using the modified kernel. To validate the modified model, the pressure field and the wave front position of the 2D dam break flow were compared with those of experimental data, the standard SPH method and the mSPH-T method, which is the turbulence SPH method without modification of the kernel and its gradients. Finally, a 3D wave impact was simulated using the mSPH-T-K method. A comparison of results with experimental data showed that this model is a powerful tool for the simulation of complicated free surface flows with large deformations and impact.

Key words: *Weakly Compressible SPH, Modification of Kernel, Modification of Kernel Gradient, 3D Wave Impact*

1. Introduction

Wave breaking and wave impact loads on coastal structures are examples of free surface flows with significant industrial and environmental importance. These phenomena may cause damage to marine structures and ships and endanger human life. Wave impact is a complicated phenomenon which causes a dramatic pressure gradient and free surface deformations. In these circumstances, the flow is rotational, viscous, and turbulent. A reliable and reasonable approach to the simulation of free surface flow involves the Navier-Stokes equations. These equations can be solved via the grid-less Lagrangian or Eulerian grid-based methods. The fixed grid solvers should be coupled with a mathematical treatment of the free surface such as the volume of fluid (VOF) method [1]. However, Lagrangian solvers could simulate the free surface flow with discontinuities and large deformations such as wave breaking without any treatment. Particle methods, such as weakly compressible Smoothed Particle Hydrodynamics (SPH) which was first introduced by Monaghan [2] for free surface flows, are Lagrangian-methods. In the weakly compressible SPH method, the fluid is assumed to be weakly compressible and the equation of state is used to estimate the pressure for each particle. Furthermore, an incompressible SPH method was developed, wherein the pressure is

directly obtained by solving a Poisson's Equation (see [3, 4]). However, solving this partial differential equation is time-consuming. The SPH method has been used for many applications such as study of pipeline scouring (e.g.[5]), dam break over a wet bed (e.g.[6]), wave propagation (e.g.[7]), wave breaking on structures (e.g. [8]), and solitary wave breaking on mild slopes (e.g.[9]). In addition, the SPH method was extended and used to deal with the complicated free surface problems by Monaghan [10].

The SPH method is now commonly used in computational fluid dynamics (CFD) and seems to be promising in predicting complex free-surface flows. However, increased flow complexity requires appropriate approaches that take into account turbulent effects. The developed turbulent models, such as explicit algebraic Reynolds stress models or large eddy simulation (LES), were adapted to the SPH method (see[11]). In addition, the sub-particle scale (SPS) turbulence model, which is derived from the LES theory, is used for modelling fluid flows with free boundaries such as water waves in SPH (see [12] and [13]). In this study, the SPS turbulence method is used for numerical simulations.

On the other hand, to increases the accuracy and stability of the weakly compressible SPH method, especially in the absence of artificial viscosity or in the presence of realistic viscous terms in momentum equations, density smoothing was proposed. This kind of smoothing helps us to reduce the fluctuations of pressure and free surface due to the application of equation of state, especially in the absence of artificial viscosity. Density smoothing was applied by Colagrossi and Landrini [8] and Dalrymple and Rogers [13] to two-dimensional cases. The former authors employed one of the methods proposed by Belytschko[14]; while the latter used a kernel correction method known as the Shepard filtering. In both cases, only the smoothing of density was applied.

Therefore, a new idea of this paper is that, in addition to density smoothing, modification of the kernel and its gradients (K) for 3D problems is also performed in the turbulence (T) weakly compressible SPH method. In order to examine the performance of the modified method (mSPH-T-K), especially regarding pressure results, it will be compared with the standard SPH method and the mSPH-T method, i.e. the weakly compressible SPH method with the laminar and SPS turbulence terms in the momentum equation with only density smoothing or without the modification of kernel and its gradients. For evaluating the accuracy of the modified method, an error analysis of pressure results and the wave front position of the dam break problem is also performed. Subsequently, using the mSPH-T-K, a 3D dam break with its impact will be simulated and compared with the results of other numerical methods.

The outline of this paper is as follows. In section 2, the governing equations and fundamentals of the SPH method are discussed. In section 3, modification of the method is clearly defined, followed by discrete formulation of governing equations. Then, the time-stepping method used to integrate the discretized equations is discussed. At the end of this section, the boundary conditions are defined. In sections 4 and 5, the results of numerical simulations are presented. Finally, some discussions and conclusions are given in section 6.

2. Problem Formulation and Methodology

In this section the governing equations and the basic fundamentals of weakly compressible SPH are discussed.

2.1 Governing Equations

The governing equations of compressible viscous fluid are continuity and momentum conservation:

$$\frac{1}{\rho}\frac{\mathrm{D}\rho}{\mathrm{D}t}+\nabla\cdot\mathbf{u}=0, \tag{1}$$

$$\frac{\mathrm{D}\mathbf{u}}{\mathrm{D}t} = -\frac{1}{\rho}\vec{\nabla}P + \mathbf{g} + \nu_0\nabla\cdot(\nabla\mathbf{u}) + \frac{1}{\rho}\vec{\nabla}\cdot\tau^*, \tag{2}$$

where ρ is the density, u is the velocity vector, P is the pressure, $\mathbf{g}$ is the acceleration vector due to gravity and $\nu_0\nabla\cdot(\nabla\mathbf{u}) + \frac{1}{\rho}\vec{\nabla}\cdot\tau^*$ are the diffusion terms in which ν_0 is the kinematic viscosity for laminar flow and τ^* is the turbulence tensor, which will be discussed in 2.4.

2.2 Basic SPH Concepts

SPH is an interpolation method developed by Monaghan [15]. In SPH, any scalar function A($\mathbf{r}$) at particle a and its gradient are approximated by:

$$\begin{cases} A(\mathbf{r}_a) = \sum_b m_b \frac{A_b}{\rho_b} W_{ab} \\ (\nabla A)_a = \rho_a \sum_b m_b \left(\frac{A_a}{\rho_a^2} + \frac{A_b}{\rho_b^2}\right)\nabla_a W_{ab} \end{cases}, \tag{3}$$

and the divergence of a vector function A($\mathbf{r}$) at particle a is interpolated by:

$$\begin{cases} \mathbf{A}(\mathbf{r}_a) = \sum_b m_b \frac{\mathbf{A}_b}{\rho_b} W_{ab} \\ (\nabla\cdot\mathbf{A})_a = -\frac{1}{\rho_a}\sum_b m_b \mathbf{A}_{ab}\cdot\nabla_a W_{ab} \end{cases}, \tag{4}$$

where $W(|\mathbf{r}_{ab}|, h)$ is the weighting or kernel function, h is the smoothing length of the kernel and $\nabla_a W_{ab} = \frac{\mathbf{r}_{ab}}{|\mathbf{r}_{ab}|}\frac{\partial W(|\mathbf{r}_{ab}|,h)}{\partial|\mathbf{r}_{ab}|}$, in which $\mathbf{r}_{ab} = \mathbf{r}_a - \mathbf{r}_b$. The summation is over all the neighbouring particles. ρ_b and m_b are the density and the mass, respectively.

The kernel function that directly affects the results of the SPH method should have specific properties such as positivity, compact support, normalization, monotonically decreasing behaviour and delta function behaviour. In this study, the cubic B-spline kernel proposed by Monaghan [16] was used, which is defined as:

$$W(|\mathbf{r}|,h) = \alpha_D \begin{cases} 1 - \frac{3}{2}q^2 + \frac{3}{4}q^3 & 0 \le q \le 1 \\ \frac{1}{4}(2-q)^3 & 1 \le q \le 2, \\ 0 & q \ge 2 \end{cases} \tag{5}$$

where $q = |\mathbf{r}|/h$ and α_D is $10/(7\pi h^2)$ for *2D* and $1/(\pi^3/2\ h^2)$ for *3D*. The second derivative of this kernel is continuous, and the dominant error term in the integral interpolant is in the order of O(h^2). A simple approach to dynamically evolving h so that the number of the neighbouring particles remains relatively constant is to update the smoothing length according to the averaged density as $h = h_0\left(\frac{\rho_0}{\rho}\right)^{\frac{1}{\dim}}$, (see [17]) where h_0 is the initial smoothing length that is taken as 1.25 times of initial particle spacing in this research, ρ_0 is the reference density that is usually taken as the density of the fluid at the free surface (ρ_0=1000 kg/m^3) and dim is the number of dimensions.

In weakly compressible SPH, pressure is calculated by the Tait equation of state defined as [18]:

$$P = B\left[\left(\frac{\rho}{\rho_0}\right)^{\gamma} - 1\right], \tag{6}$$

Where $B = c_0^2\rho_0 / \gamma$ is the bulk modulus of elasticity of the fluid, c_0 is the speed of sound at reference density which is usually taken as the density of the fluid at the free surface (ρ_0=1000 kg/m^3) and γ is a constant that equals to 7. This equation implies that the fluid is compressible, and that there is a speed of sound ($c_0^2 = \partial P/\partial\rho\big|_{\rho_0}$), which is set by changing the value of B to be approximately sixteen times of the maximum fluid velocity.

2.3 SPH Method and Artificial Viscosity

In many SPH calculations, the so-called artificial viscosity which does not have a physical meaning, proposed by Monaghan, was used to eliminate numerical diffusion in a boundary face and stabilize the calculations (e.g. Monaghan [15]; Crespo et al. [6]; Dalrymple and Rogers[13]). For this purpose, the term of Π which shows artificial viscosity is added to the right hand side of the momentum equation and has the original form as follows:

$$\Pi_{ab} = \begin{cases} -\alpha\,\bar{c}_{ab}\dfrac{\mu_{ab}}{\bar{\rho}_{ab}} & \text{for } \mathbf{u}_{ab}\cdot\mathbf{r}_{ab} < 0 \\ 0 & \text{for } \mathbf{u}_{ab}\cdot\mathbf{r}_{ab} > 0 \end{cases}, \tag{7}$$

where

$$\bar{c}_{ab} = 0.5(c_a + c_b),\ \bar{\rho}_{ab} = 0.5(\rho_a + \rho_b),\ \mathbf{u}_{ab} = \mathbf{u}_a - \mathbf{u}_b,$$
$$\mu_{ab} = h\,\mathbf{u}_{ab}\cdot\mathbf{r}_{ab} / (\mathbf{r}_{ab}^{\,2} + \eta^2),\ \eta^2 = 0.01h^2.$$

in which α is an empirical coefficient that is usually taken as 0.01–0.1. In this paper α is taken as 0.08 for the dam break test and 0.02 for the plunging wave breaking in a flume. With artificial viscosity included, the governing equations are discretized as follows:

$$\left(\frac{\mathrm{d}\rho}{\mathrm{d}t}\right)_a = \sum_b m_b(\mathbf{u}_a - \mathbf{u}_b)\cdot\nabla_a W_{ab}, \tag{8}$$

$$\left(\frac{\mathrm{d}\mathbf{u}}{\mathrm{d}t}\right)_a = -\sum_b m_b\left(\frac{P_a}{\rho_a^{\,2}} + \frac{P_b}{\rho_b^{\,2}} + \Pi_{ab}\right)\cdot\nabla_a W_{ab} + \mathbf{g}\,. \tag{9}$$

2.4 SPH Method with a SPS Turbulence Model (SPH-T)

Researchers prefer to simulate viscosity in a realistic manner. In order to adequately present the viscosity and turbulent motions of the fluid flow, especially in the case of evolution of breaking waves, laminar viscosity along with the SPS turbulent model (e.g. [12]; [13]), are replaced with artificial viscosity. Sub-particle scaling for a compressible fluid requires a special averaging methodology. Yoshizawa[19] used Favre-averaging as $\tilde{f} = \overline{\rho f} / \bar{\rho}$ where $\overline{\cdots}$ denotes an arbitrary spatial filtering. Applying the laminar and SPS models along with a flat top spatial filter to the governing equations (Eq.(1) and Eq.(2))the following equations are obtained:

$$\frac{1}{\bar{\rho}}\frac{\mathrm{D}\rho}{\mathrm{D}t} + \nabla\cdot\tilde{\mathbf{u}} = 0, \tag{10}$$

$$\frac{\mathrm{D}\tilde{\mathbf{u}}}{\mathrm{D}t} = -\frac{1}{\bar{\rho}}\bar{\nabla}\bar{P} + \mathbf{g} + \nu_0\nabla^2\tilde{\mathbf{u}} + \frac{1}{\rho}\bar{\nabla}\cdot\tau^*. \tag{11}$$

where ν_0 represents the kinematic viscosity of laminar flow and τ^* the SPS turbulent stress. In the tensor notation, it can be written as:

$$\frac{\tau^*_{ab}}{\bar{\rho}} = 2\nu_t \tilde{\mathbf{S}}_{ab} - \frac{2}{3}k\delta_{ab} - \frac{2}{3}C_I\Delta^2\delta_{ab}, \tag{12}$$

in which $\widetilde{\mathbf{S}}_{ab}$ is the Favre-filtered rate of strain tensor:

$$\tilde{\mathbf{S}}_{ab} = -\frac{1}{2}\left(\frac{\partial\tilde{\mathbf{u}}_a}{\partial\mathbf{r}_b} + \frac{\partial\tilde{\mathbf{u}}_b}{\partial\mathbf{r}_a}\right). \tag{13}$$

In addition, following Smagorinsky[20], $\nu_t = (C_S\cdot\Delta)^2\cdot|\bar{S}|$ is the turbulence eddy viscosity, C_S=0.12 the Smagorinsky constant, Δ the initial particle spacing, $\bar{S}$ the element of SPS strain tensor as in $|\bar{S}| = \left(2\tilde{S}_{ab}\tilde{S}_{ab}\right)^{1/2}$, δ_{ab} the Kronecker delta, k the SPS turbulent kinetic energy, and according to Blin[21]C_I=0.00066. The mass and momentum conservation equations in the case of SPH turbulent model can be written in the SPH notation as (see [3, 13]):

$$\left(\frac{\mathrm{d}\rho}{\mathrm{d}t}\right)_a = \sum_b m_b(\mathbf{u}_a - \mathbf{u}_b)\cdot\vec{\nabla}_a W_{ab}, \tag{14}$$

$$\begin{aligned}\left(\frac{\mathrm{d}\mathbf{u}}{\mathrm{d}t}\right)_a &= -\sum_b m_b\left(\frac{P_a}{\rho_a^2} + \frac{P_b}{\rho_b^2}\right)\cdot\vec{\nabla}_a W_{ab} + \mathbf{g} \\ &+ \sum_b m_b\left(\frac{4\upsilon_0\mathbf{r}_{ab}\vec{\nabla}_a W_{ab}}{(\rho_a+\rho_b)|\mathbf{r}_{ab}|^2}\right)\mathbf{u}_{ab} + \sum_b m_b\left(\frac{\tau_a}{\rho_a^2} + \frac{\tau_b}{\rho_b^2}\right)\cdot\vec{\nabla}_a W_{ab}.\end{aligned} \tag{15}$$

3. Modification of the Turbulence SPH Method

The standard SPH kernel does not form a partition of unity since, in general $\sum_{b=1}^{N} W_{ab}\frac{m_b}{\rho_b} \neq 1$, in which N is the number of particles. On the other hand, particles near the free surface do not have any neighbouring particles. Therefore, the kernel smoothing functions of these particles are truncated and the conditions of consistency fail. This can seriously affect the performance of the SPH method, leading to the appearance of numerical oscillations of the free surface and pressure on or near the boundaries. This can result in rapid deterioration of the numerical solution. Correction of the kernel function W_{ab} or its gradient improves the conditions of consistency. On the other hand, the main SPH formulations without artificial viscosity preserve linear momentum. But without artificial viscosity, they cannot preserve angular momentum [15]. On the other hand, in realistic applications, it is preferred to use laminar viscosity and the SPS turbulence rather than artificial viscosity. However, the viscous term in the momentum equation cannot preserve the angular momentum [4]. To clear up this problem from incompressible SPH (ISPH), Khayyer [4] used the kernel gradient correction which was introduced by Bonet and Lock [22]. However, this correction was only used for kernel gradients in the ISPH method and for laminar flow. In order to eliminate spurious oscillations at the free surface, a number of methods aiming at restoring the partition of unity of the SPH kernel functions have been developed (e.g. [23]; [24]; [14]).

In this paper, the kernel and its gradients are corrected for the weakly compressible SPH and for the turbulent flow; the modified kernel W_{ab}^m and the two modified components of the kernel gradient along the x and y and z coordinate axes, namely $(\nabla_a W_{ab}^m)_x$, $(\nabla_a W_{ab}^m)_y$, and $(\nabla_a W_{ab}^m)_z$ are expressed as:

$$\begin{bmatrix} W_{ab}^{m} \\ \left(\nabla W_{ab}^{m}\right)_x \\ \left(\nabla W_{ab}^{m}\right)_y \\ \left(\nabla W_{ab}^{m}\right)_z \end{bmatrix} = W_{ab}^{S} \underbrace{\begin{bmatrix} a_{11} & a_{12} & a_{13} & a_{14} \\ a_{21} & a_{22} & a_{22} & a_{22} \\ a_{31} & a_{32} & a_{33} & a_{34} \\ a_{41} & a_{42} & a_{43} & a_{44} \end{bmatrix}}_{Unknown\,Coefficients} \begin{bmatrix} 1 \\ x_{ab} \\ y_{ab} \\ z_{ab} \end{bmatrix}, \tag{16}$$

in which $x_{ab} = x_a - x_b$, $y_{ab} = y_a - y_b$ and W_{ab}^{S} is defined by:

$$W_{ab}^{S} = \frac{W_{ab}}{\sum_{b=1}^{N} \frac{m_b}{\rho_b} W_{ab}}. \tag{17}$$

Now, for any particle a in the domain, regardless of its position with respect to the boundary, W_{ab}^{S} represents the partition of unity since $\sum_{b=1}^{N} \frac{m_b}{\rho_b} W_{ab}^{S} = 1$. The unknown coefficients (i.e. a_{ij} , i,j=1, 2, 3,4) in Eq. (15) are determined by applying the completeness conditions for interpolating functions and their derivatives, formulated by Belytschko [14].These conditions yield the matrix equation as:

$$\mathbf{A}\,\mathbf{a}^{\mathbf{T}} = \mathbf{I}, \tag{18}$$

where $\mathbf{a}^{\mathbf{T}}$ is the matrix of unknown coefficients and $\mathbf{I}$ is the unit matrix, and $\mathbf{A}$ is given by:

$$\mathbf{A} = \sum_{b=1}^{N} \frac{m_b}{\rho_b} W_{ab}^{S} \begin{pmatrix} 1 & x_{ab} & y_{ab} & z_{ab} \\ x_{ab} & x_{ab}^2 & x_{ab}y_{ab} & x_{ab}z_{ab} \\ y_{ab} & y_{ab}x_{ab} & y_{ab}^2 & y_{ab}z_{ab} \\ z_{ab} & z_{ab}x_{ab} & z_{ab}y_{ab} & z_{ab}^2 \end{pmatrix}. \tag{19}$$

Now, the resulting modified kernel functions and their gradients given by Eq. (15) are used to replace the standard SPH counterparts in the equations of continuity and momentum, given by Eq.(13) and Eq.(14). Thus, these equations are rewritten as:

$$\left(\frac{\mathrm{d}\rho}{\mathrm{d}t}\right)_a = \sum_b m_b (\mathbf{u}_a - \mathbf{u}_b) \cdot \vec{\nabla}_a W_{ab}^{m}, \tag{20}$$

$$\begin{aligned} \left(\frac{\mathrm{d}\mathbf{u}}{\mathrm{d}t}\right)_a &= -\sum_b m_b \left(\frac{P_a}{\rho_a^{\,2}} + \frac{P_b}{\rho_b^{\,2}}\right) \cdot \vec{\nabla}_a W_{ab}^{m} + \mathbf{g} \\ &+ \sum_b m_b \left(\frac{4\upsilon_0 \mathbf{r}_{ab} \vec{\nabla}_a W_{ab}^{m}}{\left(\rho_a + \rho_b\right)\left|\mathbf{r}_{ab}\right|^2} \right) \mathbf{u}_{ab} + \sum_b m_b \left(\frac{\tau_a}{\rho_a^2} + \frac{\tau_b}{\rho_b^2}\right) \cdot \vec{\nabla}_a W_{ab}^{m}. \end{aligned} \tag{21}$$

In the next section, the time-stepping scheme for the continuity and momentum equations (i.e. Eq. (19) – (20) for the mSPH-T-K model, Eq. (13) –(14) for the mSPH-T and SPH-T model and Eq.(8) –(9) for the SPH model) is discussed.

3.1 Temporal Integration

Generally, the continuity, momentum, and position equations can be written as:

$$\begin{cases} \left(\frac{\mathrm{d}\rho}{\mathrm{d}t}\right)_a = D_a \\ \left(\frac{\mathrm{d}\mathbf{u}}{\mathrm{d}t}\right)_a = \mathbf{F}_a \\ \left(\frac{\mathrm{d}\mathbf{r}}{\mathrm{d}t}\right)_a = \mathbf{U}_a \end{cases}, \tag{22}$$

where D_a and $\boldsymbol{F_a}$ correspond to the right hand side of each continuity and momentum equation; and the term $\boldsymbol{U_a}$ represents the corrected velocity of particle a. The velocity correction is performed by the XSPH scheme which was defined by Monaghan [25] as:

$$\mathbf{U}_a = \mathbf{u}_a + \varepsilon \sum_b \frac{m_b}{\bar{\rho}_{ab}} \mathbf{u}_{ab} W_{ab}^m \ , \ \bar{\rho} = \frac{\rho_a + \rho_b}{2}, \tag{23}$$

where ε is the constant parameter with values ranging between zero and unity and which is often taken as ε =0.5. This correction keeps the particles orderly. For consistency in the mSPH-T-K method, u_a are replaced by the smoothed velocities U_a in the continuity and momentum equations, i.e. Eq.(19) and Eq.(20). However, this kind of velocity correction is used in SPH, SPH-T and mSPH-T without a modified kernel, i.e.:

$$\mathbf{U}_a = \mathbf{u}_a + \varepsilon \sum_b \frac{m_b}{\bar{\rho}_{ab}} \mathbf{u}_{ab} W_{ab} \ , \ \bar{\rho} = \frac{\rho_a + \rho_b}{2}. \tag{24}$$

In this research, a predictor-corrector scheme (see [25]) is used, in which the second order scheme in time is used in order to update the values of parameters at the time level n+1. First, the variable fields are predicted at the time level n+1/2 as follows:

$$\begin{cases} \rho_a{}^{n+1/2} = \rho_a{}^n + \dfrac{\Delta t}{2} D_a{}^n \\ \mathbf{u}_a{}^{n+1/2} = \mathbf{u}_a{}^n + \dfrac{\Delta t}{2} \mathbf{F}_a{}^n \\ \mathbf{r}_a{}^{n+1/2} = \mathbf{r}_a{}^n + \dfrac{\Delta t}{2} \mathbf{U}_a{}^n \end{cases}. \tag{25}$$

In addition, the pressure at the time n+1/2 is calculated according to Eq. (6) using density in time n+1/2:

$$P_a^{n+1/2} = B\left[\left(\frac{\rho_a^{n+1/2}}{\rho_0}\right)^{\gamma} - 1\right]. \tag{26}$$

These values are corrected using forces at the half time step:

$$\begin{cases} \rho_a{}^{n+1/2} = \rho_a{}^n + \dfrac{\Delta t}{2} D_a{}^{n+1/2} \\ \mathbf{u}_a{}^{n+1/2} = \mathbf{u}_a{}^n + \dfrac{\Delta t}{2} F_a{}^{n+1/2} \\ \mathbf{r}_a{}^{n+1/2} = \mathbf{r}_a{}^n + \dfrac{\Delta t}{2} \mathbf{U}_a{}^{n+1/2} \end{cases}. \tag{27}$$

Finally, the values are calculated at the end of time step as:

$$\begin{cases} \rho_a{}^{n+1} = 2\rho_a{}^{n+1/2} - \rho_a{}^n \\ \mathbf{u}_a{}^{n+1} = 2\mathbf{u}_a{}^{n+1/2} - \mathbf{u}_a{}^n \\ \mathbf{r}_a{}^{n+1} = 2\mathbf{r}_a{}^{n+1/2} - \mathbf{r}_a{}^n \end{cases}. \tag{28}$$

The updated pressure at time n+1 is calculated using the value of density at time n+1 as follows:

$$P_a^{n+1} = B\left[\left(\frac{\rho_a^{n+1}}{\rho_0}\right)^{\gamma} - 1\right]. \tag{29}$$

3.1.1 The variable time step

The variable time step is controlled by the Courant and viscosity conditions (see [7]). A variable time step δt is calculated as follows:

$$\delta t = \min_{a}\left(\frac{0.3h}{\mathbf{c}_a + \sigma_a}\right), \quad \sigma_{\mathbf{a}} = \max_{\mathbf{b}}\left|\frac{h\ \mathbf{u}_{ab}\cdot\mathbf{r}_{ab}}{\mathbf{r}_{ab}^{\ 2}}\right|. \tag{30}$$

where the minimum and maximum are over all particles.

3.2 Periodic Smoothing of Density

Density smoothing should be applied to smooth the unphysical behaviour at the free surface due to density variations being magnified by the equation of state when using realistic viscous terms ([8]; [13]). In this paper, density is periodically smoothed by applying the following formula every n time steps in calculations:

$$\rho_a = \sum_b m_b W_{ab}^m . \tag{31}$$

The values of n related to the Courant number were selected based on the study of Kiara [26] as presented in 0Table 1. In this paper, an analysis is performed in 4.5 to choose the appropriate values of n for pressure field. The results show that the most appropriate choices for *n* and the Courant number are 20 and μ_c =0.3, respectively.

Table 1 Minimum number of time steps and relevant Courant numbers for smoothing

Courant Number	*Minimum Number of Time Steps for Smoothing*
$\mu_c = 1$	2
$\mu_c = 0.8$	5
$\mu_c = 0.5$	15
$\mu_c = 0.1$	O(10^3)

Table 2 defines the methods which are applied in this study. SPH is the standard weakly compressible SPH method with artificial viscosity term in the momentum equation. SPH-T method is the weakly compressible SPH method with laminar and SPS turbulence terms in the momentum equation (without artificial viscosity) and without modification of density or kernel. mSPH-T is the weakly compressible SPH method with laminar and SPS turbulence terms in the momentum equation with only density smoothing. mSPH-T-K is the weakly compressible SPH method with laminar and SPS turbulence terms in the momentum equation with density smoothing and modification of the kernel and its gradients. The latter method, i.e. mSPH-T-K, is a new area of this research developed to get better results.

Table 2 Description of the SPH methods used in this paper

Method	*Artificial Viscosity*	*Laminar and Turbulence*	*Density Smoothing*	*Modification of Kernel and Gradient of Kernel*
mSPH-T-K	No	Yes	Yes	Yes
mSPH-T	No	Yes	Yes	No
SPH-T	No	Yes	No	No
SPH	Yes	No	No	No

3.3 Boundary Conditions

In this research, Dynamic Boundary Particles (DBPs) are used for all models. For fixed boundaries, these particles are constituted by fixed particles placed in a staggered grid manner [27]. The fixed particles follow the governing equations, (1) and (2), and the equation of state(6). However, they are not allowed to move based on Eq.(22). Additionally, for moving boundaries such as wave-maker, one just has to impose the position and velocity of boundary particles in each time step. This type of boundary condition is easy to apply due to its computational effortlessness as the interaction between a fluid and a boundary can be calculated inside the same loops as fluid particles. The simple repulsion mechanism of DBPs is that when a fluid particle approaches the boundary, the density of the boundary particles increases based on continuity equation, resulting in the pressure increase following Eq.(6). Thus, the force exerted on the fluid particle increases due to the pressure term P/ρ^2 in the momentum equation (i.e. Eq.(20) or Eq.(14) or Eq.(9)). More details on this subject can be found in [28].

4. 2D Dam Break Test

The flow originated by the break of a dam and the impact of the water front against a vertical wall has been used as a benchmark for the validation of the modified method. In this section, first, for the free surface validation, numerical results of the mSPH-T-K, the mSPH-T and the SPH model are compared with the experimental results of Martin [29]. At this stage, a convergence study is also conducted to choose the appropriate initial particle spacing for other numerical simulations. Furthermore, for the validation of pressure field, the results of the SPH and the mSPH-T-K method are compared with the experimental results of Hu and Kashiwagi [30]. A schematic representation of the computational domain is shown in Fig. 1. Point *A* denotes the point where a pressure sensor was installed in the wall of the experimental model.

4.1 Modelling and Simulation Condition

The dimensions of the dam break test in the experiment carried out by Martin and Moyce[29] were $L_W = a$, $H_W = 2a$, $L_d = 4a$ where $a = 5.7$ cm. The dimensions of the dam break test in the experiment carried out by Hu and Kashiwagi [30] were $L_W = 68$ cm, $H_W = 12$ cm and $L_d = 118$ cm .The initial size of particle spacing is chosen as $\mathrm{d}x = \mathrm{d}y = 0.005$ m.

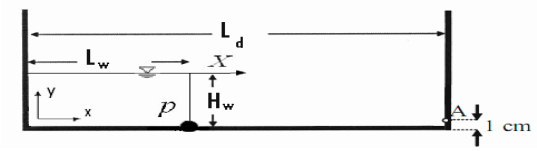

Fig. 1 Schematic representation of the dam break benchmark

4.2 Free Surface Validation

After the initiation of water column slumping, the position of the water front edge particle p was recorded along the tank before it collided with the right wall of the domain. The results were compared with the numerical VOF results (see [1]) and the experimental data (see [29]), as shown in Fig. 2. In this figure, *X* is the longitudinal coordinate from point p. As it can be seen, the results of the mSPH-T-K method are closer to the experimental data than those of the VOF method and those of SPH or mSPH-T. To quantify the comparison between the experimental and the presented numerical results, two statistical parameters of *M* and N are used as follows:

$$M = \sqrt{\sum_{i=1}^{ne}(Val_i^{simulation})^2 \Big/ \sum_{i=1}^{ne}(Val_i^{\exp})^2}\,, \tag{32}$$

$$N = \sqrt{\sum_{i=1}^{ne}(Val_i^{simulation} - Val_i^{\exp})^2 \Big/ \sum_{i=1}^{ne}(Val_i^{\exp})^2}\,, \tag{33}$$

in which $Val_i^{simulation}$ and $Val_i^{\exp}$ are the numerical and experimental values respectively and ne is the number of experimental data. Good agreement between the results of the experiment and of the model should result in $M \rightarrow 1$ and $N \rightarrow 0$. Table 3 clearly shows that the results of the mSPH-T-K method are more accurate than those of other methods.

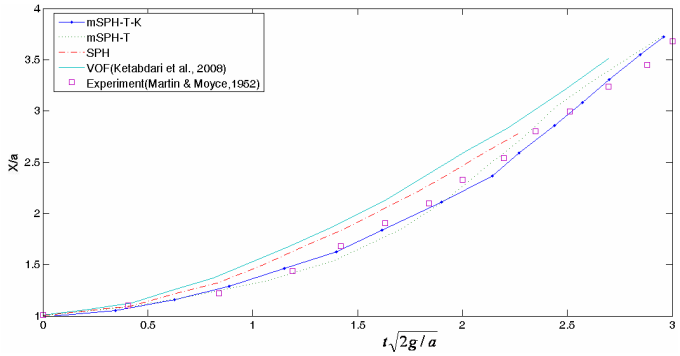

Fig. 2 Comparison of non-dimensional results of longitudinal position of point p along the tank versus time in the dam break test (Point *p* is the water front edge particle during simulation (See Fig. 1)).

Table 3 Calculated values of *N* and *M* in four different methods for the longitudinal position of point *p* (See Fig. 1)

Case	*SPH*	*mSPH-T*	*mSPH-T-K*	*VOF*
M	1.014	0.989	1.005	1.019
N	0.084	0.065	0.032	0.091

4.3 Convergence Study of the mSPH-T-K Method

In order to see how the accuracy of mSPH-T-K results varies with increasing the number of particles, a convergence analysis of the dam break simulation results was carried out, as shown in Fig. 2. Thus, two additional calculations with coarser (d = 0.01 m) and finer (d = 0.0025 m) particle spacing were performed. In Fig. 3 one can clearly see that the results converge to the experimental data as the particle distances are reduced and more computational particles are employed. The difference between the results corresponding to d = 0.005 m and d = 0.0025 m is much smaller than that seen between the results with d = 0.005 m and d = 0.01 m. Considering both the accuracy and the computational effort, the particle spacing of d = 0.005 m is selected as an optimum value.

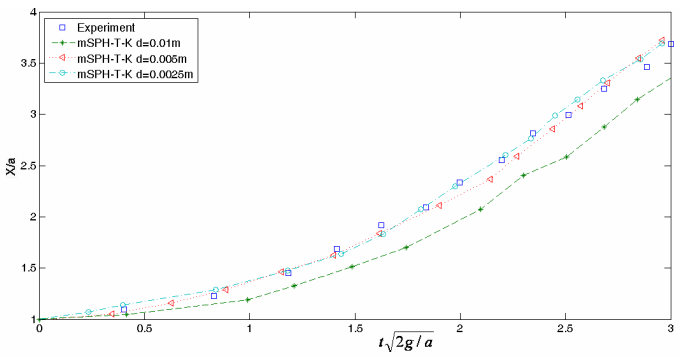

Fig. 3 Convergence study of results presented in Fig. 2 by decreasing the particle spacing in the mSPH-T-K method

4.4 Comparison of Pressure Field in the SPH, SPH-T, mSPH-T and mSPH-T-K methods

Fig. 4 shows photographs of water particles together with the pressure distribution in different SPH models at t=0.0, 0.33, 0.7 and 0.9 seconds. In this figure, the first (from the left), second, third and fourth columns are related to the SPH, SPH-T, mSPH-T and mSPH-T-K methods, respectively. It can be seen that the pressure distribution of the SPH and the SPH-T method (except at t=0.00 s) is spurious and irregular. Furthermore, the free surface of the SPH-T method, unlike that of the SPH method, is unphysical and the particle scattering occurs. On the other hand, the pressure distribution and the free surface of the mSPH-T and mSPH-T-K methods are appropriate and normal. However, the free surface of mSPH-T-K is much better than that of mSPH-T, especially at t=0.9 s. In fact, modification of the kernel and its gradient in mSPH-T-K results in a better reproduction of the plunging jet and splash-up processes at t=0.9s. However, it is seen that the splash-up process is not reproduced in the mSPH-T method at t=0.9s. Thus, it is concluded that the modification of the kernel and its gradient with density smoothing is more effective than only density smoothing for complex free surface simulations such as splash-up process. At the beginning of the calculations, all models have similar pressure distribution.

After the beginning of the calculation (t=0.0 s), the dam break flow is characterized by the development of a tongue of water spreading along the horizontal boundary (t=0.33 s). Later on, this tongue of water strikes the vertical wall producing a high impact pressure. After the impact at t=0.7 s, the water moves upwards and rises up the wall in the form of a jet. In rising up the wall, the jet slows down under the restoring action of gravity and starts to reverse. Eventually, due to the oncoming flow, at t=0.9 s, the jet overturns in the form of a plunging wave and hits the underlying water and produces a splash-up. It is seen that the plunging jet, the bubble capturing and the splash-up process are well simulated by mSPH-T-K at t=0.7 and t=0.9 s. However, at these stages, the free surfaces of mSPH-T and SPH are not as good as that of the mSPH-T-K method. As a matter of fact, the mSPH-T-K method can only simulate the nonlinear free surface due to the modification of the kernel and the kernel gradient to preserve the angular momentum .This shows the efficiency of the mSPH-T-K method in the simulation of highly non-linear processes with non-linear strain rate of flow due to the employment of tensor-type realistic laminar and turbulence viscosity.

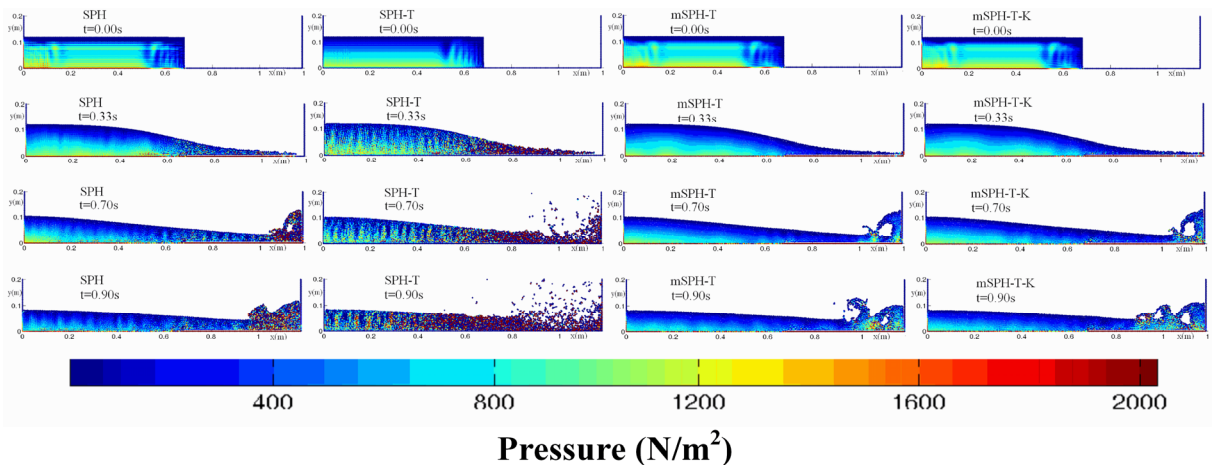

Fig. 4 Pressure distribution in the dam break of SPH models; from the left, first column - standard SPH method, second column - SPH-T, i.e. the SPH method with a turbulence model, third column - mSPH-T, i.e. the SPH method with a turbulence model and density smoothing, and fourth column - the modified method, i.e. mSPH-T-K

4.5 Validation of Pressure Values

Fig. 5 compares the time histories of pressure at point A in Fig. 1 with experimental results. The pressure results were evaluated using the SPH, mSPH-T and mSPH-T-K methods. It can be seen that the SPH results exhibit large fluctuations and are highly overestimated. However, pressure fluctuations of the mSPH-T results are much less pronounced than those of SPH due to the periodic smoothing of density. However, the results are highly overestimated. Finally, the mSPH-T-K results are rather accurate in comparison with experimental data due to the density smoothing and modification of the kernel and its gradients. This method is good at estimating the first and second peaks. However, the first peak in mSPH-T-K occurs at 0.38 s and its value is 1726 N/m^2, while the time and the maximum pressure value of the experiment are 0.35s and 1570 N/m^2 respectively. This demonstrates an overestimation of about 10%. Also, the second pressure peak time and its value in the experiment are 0.75 s and 1230 N/m^2 respectively, while those of mSPH-T-K are 0.79 s and 972 N/m^2. This shows an underestimation of about 20%.

Fig. 6 shows the relative error in pressure results of the mSPH-T-K and mSPH-T methods as $\frac{|P_N - P_E|}{P_E}$ in which P_E and P_N are the experimental and numerical pressure results, respectively. The horizontal lines in Fig. 6 show the mean value of relative error in each method. It can be seen that the mean value of relative error of mSPH-T is about 1.19, while that of the modified method is about 0.25. Thus, the modified method gives appropriate pressure results, unlike the SPH and mSPH-T methods.

Fig. 7 shows the pressure results of mSPH-T-K with four values of smoothing in comparison with experimental results. It can be seen that the numerical results for n=10 are highly overestimated. It is also evident that the best results can be obtained with n=20. However, the results for n=30 and n=40 have dramatic fluctuations around the first peak pressure.

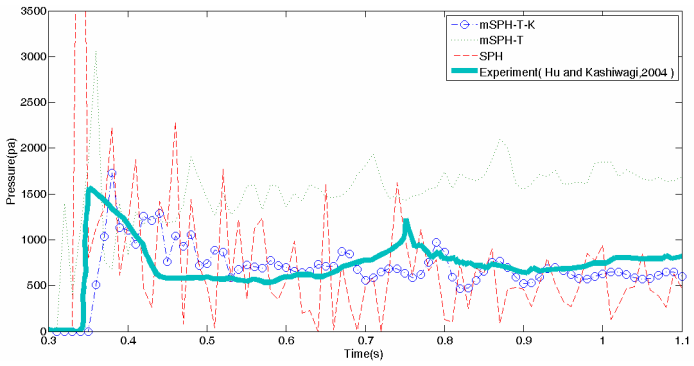

Fig. 5 Time histories of calculated pressure at point *A* in the dam break with impact test using the standard and modified SPH methods

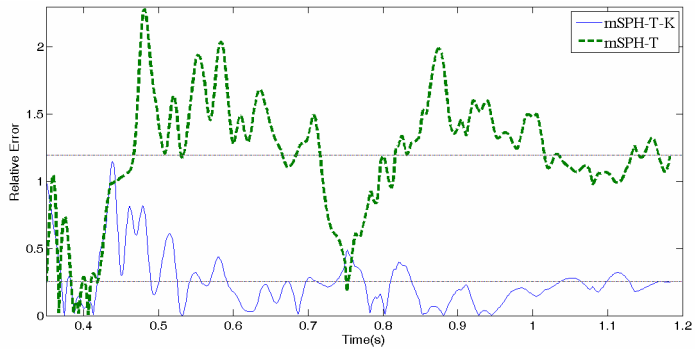

Fig. 6 Relative error in the pressure results of the mSPH-T-K and mSPH-T methods

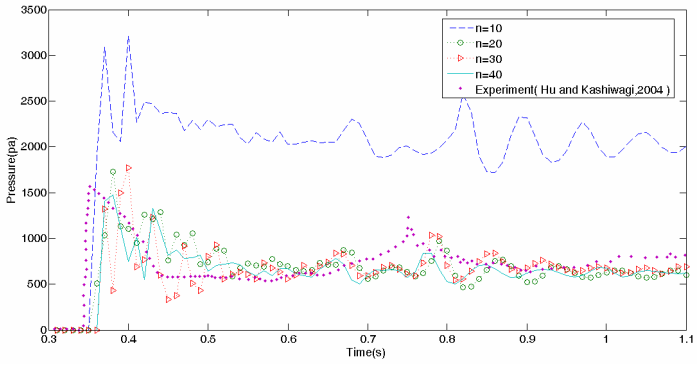

Fig. 7 Time histories of calculated pressure at point A in the dam break with impact test using the mSPH-T-K method with different values of the number of periodic smoothing (n)

5. 3D Dam Break with Impact

The second benchmark is based on the experimental configuration of Kleefsman et al. [31] in which a rectangular box is located in an open roof tank (See Fig. 8). The geometry and the measurement positions are briefly described in Fig. 8. In this figure points H1 to H4 are used to observe the water heights while P1 to P8 are pressure sensors on the box. In this experiment, water is held by a gate and released as the gate is pulled up instantly. In the numerical study, instead of modelling the gate motion, the water is released immediately. In the numerical simulation, the artificial speed of sound is C=13u_{max}=28m/s and the particle spacing is considered as $\mathrm{d}x = \mathrm{d}y = 0.005$ m.

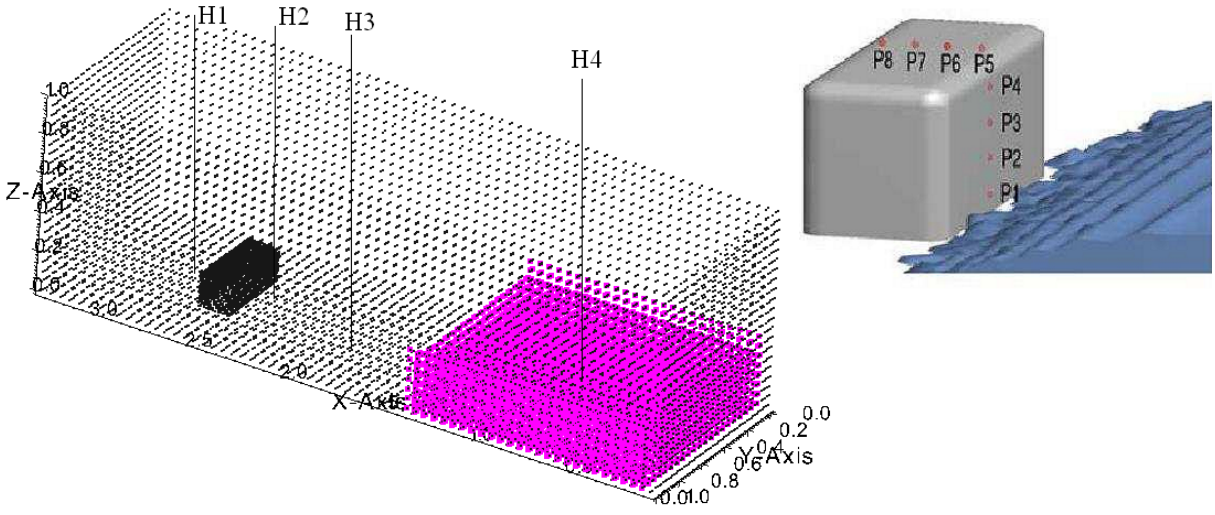

Fig. 8 Schematic representation of the numerical simulation of dam break with a box

5.1 Comparison between Different SPH Methods

Fig. 9 shows photographs of water particles together with the distribution of pressure in different SPH models at t=0.42, 0.64, 1.26, 1.44 and 2.08 seconds. It is mentioned that α=0.012 is the coefficient of artificial viscosity in the SPH method. At t=0.42 s the dam break flow is characterized by the development of a tongue of water spreading along the horizontal boundary. Later on, this tongue of water strikes the box (t=0.64 s) producing a high impact pressure. After the impact, the water moves upwards along the box in the form of a jet. In

moving upwards along the box, the jet overtops the box and creates a plunging jet under the restoring action of gravity (t=1.26 s). At this stage, the breaking wave comes toward the wall and strikes the vertical wall (t=1.44 s) producing a high impact pressure. Later on, a plunging jet forms and this jet slows down under the restoring action of gravity and starts to reverse. Then a plunging wave breaker is generated and the wave again overtops the box (t=2.08 s). It can be seen from Fig. 9 that the pressure distribution in the SPH method is irregular and spurious, while the pressure distributions in mSPH-T and mSPH-T-K are smooth and regular. However, the pressure distribution in mSPH-T-K is smoother than that in mSPH-T. Furthermore, the bubble capturing does not occur in SPH.

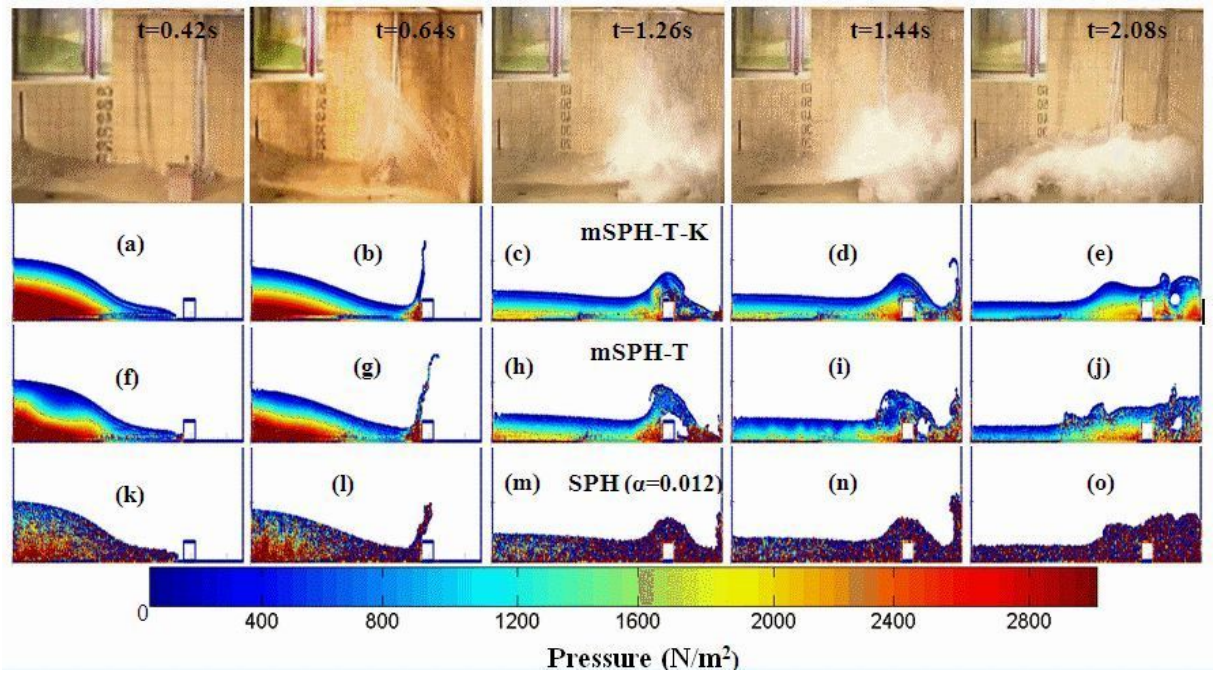

Fig. 9 Pressure distribution in the dam break with impact in different SPH models at t=0.42, 0.64, 1.26, 1.44 and t=2.08 seconds (side view)

5.2 Validation of Pressure Values

Fig. 10 compares the time histories of pressure at measuring points on the box, P1, P3, P5 and P7.These time histories include the results of experiment, the VOF simulation [31], SPH, mSPH-T, and mSPH-T-K. As one can see, the SPH results have large fluctuations and are highly overestimated, while large fluctuations in mSPH-T and mSPH-T-K are eliminated. However, mSPH-T-K, unlike mSPH-T, produces reasonably good results in comparison with experimental data. For this reason, the pressure results of the SPH method are not included in Fig. 10 (c)-(d). However, it can be seen from Fig. 10 (a)-(d) that the results of VOF are also overestimated at t=1.2 s and t=4.7 s. It is noted that mSPH-T-K, unlike mSPH-T, predicted the first and the second peak of pressure results. Furthermore, the results of mSPH-T in Fig. 10 (a) are overestimated and underestimated in Fig. 10 (b)-(c). For a more precise comparison of the mSPH-T and mSPH-T-K results and experimental results, two statistical parameters of M and N are calculated for P1, P2, P3 and P4 in Table 4. It is mentioned that perfect agreement between the experiment and the numerical model will be reached when $A \rightarrow 1$ and $S \rightarrow 0$.

(a)

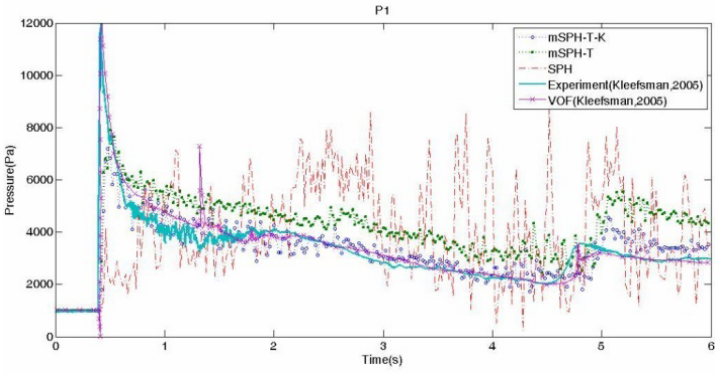

(b)

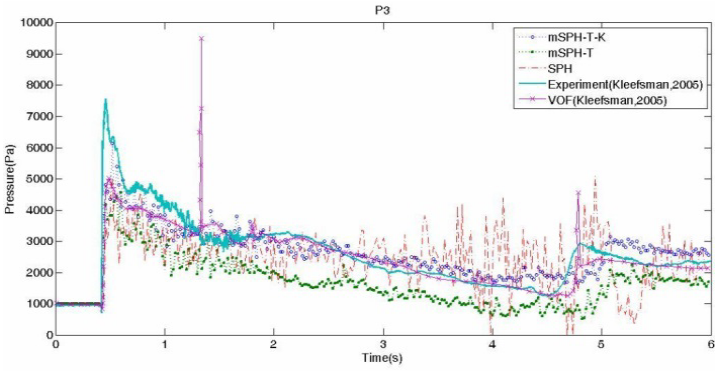

(c)

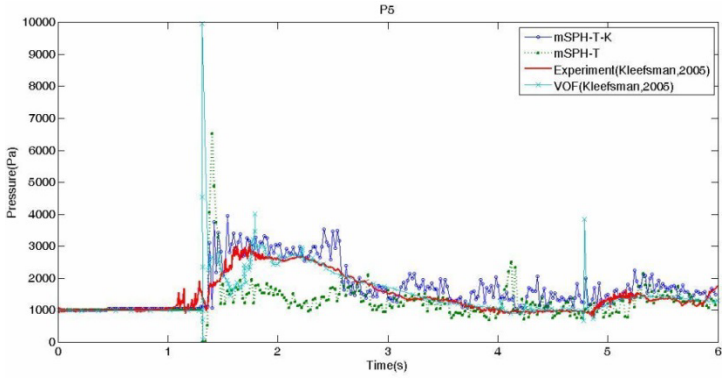

(d)

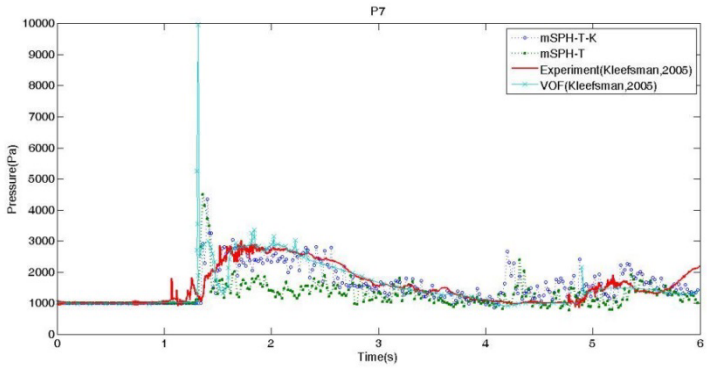

Fig. 10 Time histories of pressure at measuring points a) P1, b) P3 c) P5 and d) P7

Table 4 Calculated values of M and N for pressure results in four different methods

Case	*SPH*	*mSPH-T*	*mSPH-T-K*
M	1.41	0.89	0.98
N	0.71	0.40	0.26

5.3 Validation of Water Height Values

Fig. 11 (a and b) compares the time histories of water height at measuring points on the box, H4 and H2. These time histories include the results of the experiment, VOF, and mSPH-T-K. 0 Fig. 11 (a) shows the water height at H4. It can be seen that mSPH-T-K computes rather accurately the first and the second peak of water height. However, mSPH-T-K estimates the time of the second water height peak with a time lag of 0.3 seconds. 0Fig. 11 (b) shows the water height at H2. Although mSPH-T-K underestimates the second peak wave height, the method follows the experimental values in the same manner, with a time lag.

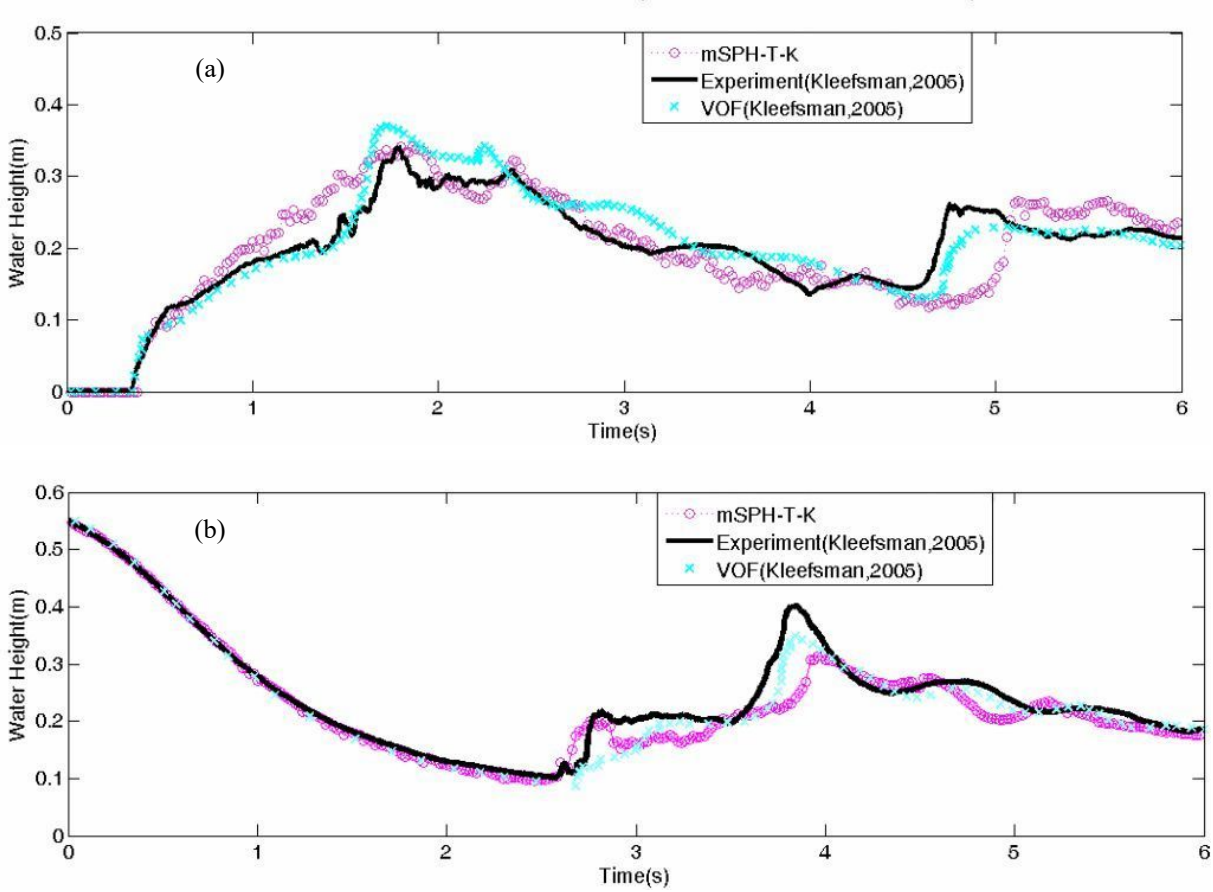

Fig. 11 Time histories of water height at measuring points a) H4 and b) H2

6. Conclusions

In this paper, the turbulence weakly compressible SPH model was modified to correct the pressure field and surface tracking. The previous studies show that using the SPS turbulence method (T) in SPH instead of artificial viscosity leads to the unphysical free surface and spurious pressure field. Therefore, in this research, some modifications were made to the SPH model to overcome these problems. Firstly, the kernel and its gradients were modified (K) in the turbulence SPH model. Secondly, the densities of particles were smoothed by means of the modified kernel. It should be mentioned that the new idea presented in this paper is the mSPH-T-K model which differs from the mSPH-T in the modification of kernel and its gradient. However, both of these methods used density smoothing. To validate the modified model, namely the mSPH-T-K, two benchmark tests were performed and the results were compared with results of the experiment and other

numerical methods. The results showed that the modified models not only reproduce well the complex free surfaces such as plunging wave breaking, but also give appropriate pressure results, unlike the standard SPH and mSPH-T methods. As a matter of fact, when using the realistic viscous terms in momentum equations, the periodic smoothing of density is required to simulate the free surface accurately However, based on the results of this paper, to obtain an accurate pressure field and better simulation of the complex free surfaces such as plunging breaking and splash-up processes, modification of the kernel and its gradient must be implemented in the model together with density smoothing.

REFERENCES

[1] Ketabdari, M.J., M.R.H. Nobari, and M.M. Larmaei. Simulation of waves group propagation and breaking in coastal zone using a Navier–Stokes solver with an improved VOF free surface treatment. Appl. Ocean Res. **30**(2) (2008).

[2] Monaghan, J.J. *Simulating free surface flows with SPH.* J. Comput. Phys. **110**: p. 399-406 (1994).

[3] Lo, E.Y.M. and S. Shao. *Simulation of near-shore solitary wave mechanics by an incompressible SPH method.* Appl. Ocean Res. **24** (2002).

[4] Khayyer, A., H.Gotoh, and S.D. Shao. *Corrected incompressible SPH method for accurate water surface tracking in breaking waves.* Coast. Eng. **55**(3): p. 236–250 (2008).

[5] Mirmohammadi, A. and M.J. Ketabdari. *Numerical simulation of wave scouring beneath marine pipeline using Smoothed Particle Hydrodynamics* Int. J. Sediment Transp. **26**(2011): p. 331-342 (2011).

[6] Crespo, A.J.C., M. Gomez-Gesteira, and R.A. Dalrymple. *Modeling dam break behavior over a wet bed by a SPH technique.* J. Waterw. Port Coast. Ocean Eng. **134**(6): p. 313-320 (2008).

[7] Monaghan, J.J. and A. Kos. *Solitary waves on a Cretan beach.* J. Waterw. Port Coast. Ocean Eng. **125**(3) (1999).

[8] Colagrossi, A. and M. Landrini. *Numerical simulation of interfacial flows by smoothed particle hydrodynamics.* J. Comput. Phys. **191**(2) (2003).

[9] Shao, S. and H. Gotoh. *Turbulence particle models for tracking free surfaces.* J. hydraul. res. **43**(3) (2005).

[10] Monaghan, J.J. *Smoothed particle hydrodynamics.* Rep. Prog. Phys. **68**: p. 1703-1759 (2005).

[11] Violeau, D. and R. Issa. *Numerical modelling of complex turbulent free-surface flows with the SPH method: an overview.* Int. J. Numer. Methods in Fluids **53**(2) (2007).

[12] Gotoh, H., T. Shibihara, and M. Hayashi. *Sub-particle-scale model for the MPS method-Lagrangian flow model for hydraulic engineering.* Comput. Fluid Dyn. J. **9**(4): p. 339-247 (2001).

[13] Dalrymple, R.A. and B.D. Rogers. *Numerical Modeling of Water Waves with the SPH Method.* Coast. Eng. **53**(2-3): p. 141-147 (2006).

[14] Belytschko, T., Y. Krongauz, J. Dolbow, and C. Gerlach. *On the completness of meshfree particle methods.* Int. J. Numer. Meth. Eng. **43**(5): p. 785–819 (1998).

[15] Monaghan, J.J. *Smoothed particle hydrodynamics.* Annual Rev. Astron. Appl. **30** (1992).

[16] Monaghan, J.J. and J.C. Lattanzio. *A Refined Method for Astrophysical Problems.* Astron. and Astrophys. **149** (1985).

[17] Liu, G.R. and M.B. Liu. *Smoothed particle hydrodynamics: a meshfree particle method*: World Scientific (2003).

[18] Batchelor, G.K. *Introduction to Fluid Dynamics*, Cambridge Cambridge Univ. Press(1967).

[19] Yoshizawa, A. *Statistical theory for compressible turbulent shear flows, with the application to subgrid modeling.* Phys. of Fluids. **29** (1986).

[20] Smagorinsky, J. *General circulation experiments with the primitive equations.* Monthly weather review. **91**(3): p. 99–164 (1963).

[21] Blin, L., A. Hadjadj, and L. Vervisch. *Large eddy simulation of turbulent flows in reversing systems.* J. Turbul. **4** (2003).

[22] Bonet, J. and T.-S.L. Lok. *Variational and momentum preservation aspects of Smoothed Particle Hydrodynamic formulations.* Comput. Methods Appl. Mech. **180**: p. 97-115 (1999).

[23] Dilts, G.A. *Moving-Least–Squares-Particle Hydrodynamics – I. Consistency and stability.* Int. J. Numer. Meth. Engng. **44** (1999).

[24] Bonet, J. and S. Kulasegaram. *Correction and stabilization of smoothed particle hydrodynamics methods with applications in metal forming simulations.* Int. J. Numer. Meth. Eng. **47**(6): p. 1189–1214 (2000).

[25] Monaghan, J.J. *On the problem of penetration in particle methods.* Journal of Computational Physics. **82**(1) (1989).

[26] Kiara, A., *Analysis of the Smoothed Particle Hydrodynamics method for free surface flows*, in *Massachusetts Institute of Technology*. 2010.

[27] Dalrymple, R.A. and O. Knio. *SPH modeling of water waves.* ASCE, (2001).

[28] Crespo, A.J.C., M. Gómez-Gesteira, and R.A. Dalrymple. *Boundary conditions generated by dynamic particles in SPH methods.* CMC-TECH SCI. PRESS. **5**(3) (2007).

[29] Martin, J.C. and W.J. Moyce. *Part IV. An Experimental Study of the Collapse of Liquid Columns on a Rigid Horizontal Plane.* Philos. Trans. Royal Soc. London. Series A, Math. Phys. Sci. **244**(882): p. 312 (1952).

[30] Hu, C.H. and M. Kashiwagi. *A CIP Method for Numerical Simulations of Violent Free Surface Flows.* J. Mar. Sci. Tech. **9**(4): p. 143-157 (2004).

[31] Kleefsman, K.M.T., G.Fekken, A.E.P. Veldman, B. Iwanowski, and B. Buchner. *A Volume of Fluid based simulation method for wave impact problems.* J. Comput. Phys. **206**: p. 363–393 (2005).

Submitted: 28.4.2014

Accepted: 28.01.2016

Mahmoud Rostami Varnousfaaderani
Faculty of Marine Technology, Amirkabir University of Technology Tehran, Iran
Mail: Rostamivf@aut.ac.ir

Mohammad Javad Ketabdari
Faculty of Marine Technology, Amirkabir University of Technology Tehran, Iran
Tel.: +98 21 6641302; Fax: +98 21 66412495 E-mail: Ketabdar@aut.ac.ir